Computational and Structural Biotechnology Journal 20 (2022) 4921–4929

COMPUTATIONAL ANDSTRUCTURAL BIOTECHNOLOGY JOURNAL

journal homepage: www.elsevier.com/locate/csbj

Structural studies of the coiled-coil domain of TRIM75 reveal a tetramer architecture facilitating its E3 ligase complex

Xiaohua Lou [a], Binbin Ma [a], Yuan Zhuang [a], Xiang Xiao [a], Laurie J. Minze [a], Junji Xing [a], Zhiqiang Zhang [a,b], Xian C. Li [a,b,*]

[a] Immunobiology and Transplant Science Center and Department of Surgery, Houston Methodist Research Institute, Houston, TX, USA
[b] Department of Surgery, Weill Cornell Medical College of Cornell University, NY, USA

ARTICLE INFO

Article history:
Received 20 June 2022
Received in revised form 29 August 2022
Accepted 30 August 2022
Available online 5 September 2022

Keywords:
Coiled-coil domain
Crystal structure
Disulfide bond
Tetramerization
TRIM75
Ubiquitin E3 ligase

ABSTRACT

Protein ubiquitination plays a vital role in controlling the degradation of intracellular proteins and in regulating cell signaling pathways. Functionally, E3 ubiquitin ligases control the transfer of ubiquitin to the target substrates. As a major family of ubiquitin E3 ligases, the structural assembly of RING E3 ligases required to exert their ubiquitin E3 ligase activity remains poorly defined. Here, we solved the crystal structure of the coiled-coil domain of TRIM75, a member of the RING E3 ligase family, which showed that two disulfide bonds stabilize two antiparallel dimers at a small crossing angle. This tetrameric conformation confers two close RING domains on the same side to form a dimer. Furthermore, this architecture allows the RING dimer to present ubiquitin to a substrate on the same side. Overall, this structure reveals a disulfide bond-mediated unique tetramer architecture and provides a tetrameric structural model through which E3 ligases exert their function.

1. Introduction

Protein ubiquitination is a post-translational modification process that controls a variety of cellular process [1]. Ubiquitinated proteins are degraded through the proteasome pathway, which controls the degradation of most intracellular proteins [2]. They are also involved in cell signaling during inflammation, DNA repair, translation, and endocytic trafficking processes [3]. Three types of enzymes act sequentially during protein ubiquitination: E1 ubiquitin-activating enzyme, E2 ubiquitin-conjugating enzyme, and E3 ubiquitin ligases. E3 ubiquitin ligases transfer the ubiquitin group from E2 to the target protein substrates. Based on their characteristic domains and ubiquitin transfer mechanisms, E3 ligases are classified into three major types: homologous to the E6-AP carboxyl terminus (HECT) type E3 ligases (approximately 30 members in humans), RING-in-between-RING (RBR) E3 ligases (approximately 12), and RING E3 ligases (approximately 600) [4]. As the majority of ubiquitin E3 ligases, RING E3 ligases need to form RING dimers to recruit the E2-Ub complex [5,6]. Therefore, the assembly of these RING-domain monomer proteins in a manner that satisfies this prerequisite is crucial for their E3 ligase activities.

The tripartite motif proteins (TRIM) constitute the largest family of RING E3 ligases with over 80 members in humans [7]. They play crucial roles in various physiological and pathological processes including DNA repair, apoptosis, autophagy, innate immunity, cell proliferation and development, and carcinogenesis [7–9]. Their dysregulation causes various diseases including cancer, infectious inflammatory, cardiovascular diseases, and neuropsychiatric disorders [10–12]. TRIM proteins usually consist of a conserved *N*-terminal tripartite motif: RING domain, B box (B box1 and/or B box 2), and coiled-coil domain, and a diverse C-terminal domain that determines substrate specificity. As a general feature of RING-type E3 ligases, dimerization of the RING domain is required for TRIM proteins to recruit the E2-Ub complex [13–15]. Structural studies have indicated that protein fragments containing the coiled-coil domain and some part of the C-terminal domain may form antiparallel dimers in TRIM5 [16], TRIM20 [17], TRIM25 [18,19], and TRIM69 [20]. Because of this antiparallel arrangement, the location of the two RING domains at opposite ends of the dimer is not conducive to dimer formation. Therefore, the assembly of TRIM proteins for exerting their E3 ligase activity remains unclear.

In this study, we solved the crystal structure of mouse TRIM75, which belongs to the largest subfamily of TRIM proteins [7], and

* Corresponding author at: Immunobiology and Transplant Science Center and Department of Surgery, Houston Methodist Research Institute, Houston, TX, USA.
E-mail address: xcli@houstonmethodist.org (X.C. Li).

https://doi.org/10.1016/j.csbj.2022.08.069

revealed the structural requirements for its RING E3 ligase activities involving the formation of tetramers to direct ubiquitin transfers to substrates.

2. Materials and methods

2.1. Phylogenetic analysis

Phylogenetic analyses were performed using MEGA 11 software [21]. The amino acid sequences of mouse TRIM proteins obtained from the UniProt database were first aligned using the MUSCLE algorithm. The resulting alignment file was used to construct a neighbor-joining (NJ) tree with the default parameters.

2.2. Cloning, expression, and purification of recombinant proteins

DNA encoding the mouse TRIM75 (UniProt code: Q3UWZ0) protein fragment 168–222 was amplified using PCR. The gene fragment was cloned into a pET28-based vector containing *N*-terminal His_6-MBP tandem tags, followed by an HRV-3C protease cleavage site. The construct was then transformed into *Escherichia coli* BL21(DE3) cells. The construct-containing cells were selected using kanamycin and grown in an LB medium at 37 °C until the OD_{600} reached 0.4; the protein was then induced overnight at 18 °C using 0.5 mM isopropyl-β-D-1-thiogalactopyranoside. The cells were harvested by centrifugation and lysed by sonication in 500 mM NaCl, 20 mM imidazole, and 20 mM Tris pH 8.0. The cell lysate supernatant obtained by ultracentrifugation was loaded onto a 5-ml Histrap HP column (GE Healthcare); the elute from the Histrap HP column was continually purified using a 5-ml MBPtrap column (GE Healthcare) according to the manufacturer's instructions. The protein eluted from the MBPtrap column was digested overnight with HRV-3C protease in a cold room. Then, the digested sample was passed over a 5 ml Histrap column to remove the His_6-MBP tandem tags. After tag removal, the sample was further purified by size-exclusion chromatography using a Superdex 200 column (GE Healthcare).

2.3. Crystallization and structure determination

Crystallization was screened by vapor diffusion using a 1:1 vol ratio of 8 mg/ml protein to crystallization reagent. Crystals were obtained under the following condition: 0.1 M Acetate pH 4.6, 20% isopropanol, and 0.2 M calcium chloride. Single crystals were frozen in mother liquor containing 20% (v/v) glycerol. Diffraction data were collected on beamline 24-ID-E at the Advanced Photon Source (Chicago, IL, USA) at 0.97918 Å wavelength. The collected data were processed using Imosflm and AIMLESS [22,23]. The structure was solved by molecular replacement with a search model of 40-alanine alpha helix using Phaser [24]. The initial model was subjected to rounds of refinement using REFMAC5 [25] and Coot software [26] was used to monitor and correct the model after refinement. The structural figures were generated with PyMol (Schrödinger, LLC). The crystal structure results are presented in Table 1.

2.4. TRIM75 mutagenesis

Mutants of full-length TRIM75, TRIM75 protein fragment containing coiled-coil domain and C-terminal domain, and TRIM75 coiled-coil domain were produced using site-directed mutagenesis. The results were confirmed by sequencing.

Table 1
Data collection and refinement statistics.

Data collection	
X-ray source	24-ID-E
Wavelength(Å)	0.97918
Space group	$I4_122$
Cell dimensions	
a, *b*, *c* (Å)	43.07, 43.07, 134.32
Resolution[a] (Å)	8.00–2.05 (2.16–2.05)
No. of unique reflections	4039
Completeness (%)	96.3(99.6)
Redundancy	3.2(3.3)
R_{merge} (%)[b]	4.2(24.8)
$I/\sigma I$	14.1(4.2)
CC (1/2)	0.998(0.913)
R_{pim} (%)[c]	2.6(15.4)
Refinement	
Resolution (Å)	7.99–2.05
R_{work}/ R_{free} (%)[d]	21.14/25.62
R.m.s deviations	
Bond lengths (Å)	0.010
Bond angles (°)	1.806
Ramachandran	
Favored (%)	100
Allowed (%)	0
No. of non-H atoms	
Protein	457
Ligand	10
H_2O	30
Average B factors (Å^2)	
Protein	53.3
Ligand	56.0
H_2O	55.9

[a] Values for the outer shell are given in parentheses.
[b] $R_{merge} = \Sigma_{hkl}\Sigma_i |I_i(hkl) - < I(hkl) >| / \Sigma_{hkl} \Sigma_i I_i(hkl)$, where $I_i(hkl)$ is the intensity of reflection i and $< I(hkl) >$ is the average intensity of all reflections with indices hkl.
[c] $R_{pim} = \Sigma_{hkl} [1/(N-1)]^{1/2} \Sigma_i |I_i(hkl) - < I(hkl) >| / \Sigma_{hkl} \Sigma_i I_i(hkl)$.
[d] $R_{work} = \Sigma_{hkl} || F_{obs}(hkl)| - |F_{calc}(hkl)|| / \Sigma_{hkl} |F_{obs}(hkl)|$; R_{free} was calculated using 8% of data.

2.5. SEC-MALS assay

The molar mass of the coiled-coil domain of TRIM75 protein in solution was measured using SEC-MALS in the Core for Biomolecular Structure and Function (CBSF) at the University of Texas MD Anderson Cancer Center, Houston, Texas. The MALS system was equipped with a WTC-010S5 column (Wyatt Technology Co. ltd), a differential refractive index detector, and an 18-angle static scattering detector. The system was calibrated using BSA. The purified protein (40 μl) at a concentration of 5 mg/ml was loaded for the run at room temperature. Phosphate-buffered saline (PBS) was used as the running buffer. Data were recorded and analyzed using ASTRA software (Wyatt Technology).

2.6. Chemical cross-linking assay

For the coiled-coil domain, the purified protein in PBS with or without DTT was used for the cross-linking assay. Glutaraldehyde (GA) (Sigma-Aldrich) was added from freshly prepared 0, 10, 20, 40, and 80 mM stocks in PBS to five samples with final concentrations of 0, 1, 2, 4, and 8 mM, respectively. The samples were then incubated at room temperature for five minutes and then terminated by adding an equal volume of saturated glycine solution at room temperature [27,28]. The cross-linked samples were resolved on 4–15% Mini-PROTEAN TGX Precast Protein Gels (Bio-Rad), and the gel was stained with Coomassie Brilliant Blue R-250.

For full-length or truncated proteins, a gene (Uniprot code: Q3UWZ0) with an *N*-terminal FLAG tag was cloned into the pBudCE4.1 (Invitrogen) vector multiple cloning site (MCS) region

using the CMV promoter. For plasmid transfection, 15 μg of DNA was transfected into 4×10^6 HEK293T cells in a 100 mm dish using Lipofectamine 3000 (Invitrogen) according to the manufacturer's protocol. After two days of incubation, the cells were washed with PBS and lysed in RIPA buffer with EDTA-free protease inhibitor cocktail (Roche) on ice. The target protein was extracted with anti-FLAG Magnetic Agarose (Pierce) from the clear cell lysate. Then, the agarose was washed three times with a washing buffer containing 20 mM tris pH7.5, 500 mM NaCl, 0.5% TWEEN 20, and EDTA-free protease inhibitor cocktail. 1X FLAG peptide (0.2 mg/ml) in PBS with EDTA-free protease inhibitor cocktail was used to elute FLAG-tagged proteins. The FLAG peptide was removed from the eluate via centrifuge with an Amicon 10 K MWCO centrifugal filter. All procedures were done in a cold room. The final sample in PBS with EDTA-free protease inhibitor cocktail was aliquoted into five tubes for the cross-linking experiments. After cross-linking, freshly quenched samples were immediately resolved on 4–15% Mini-PROTEAN TGX Precast Protein Gels (Bio-Rad) and visualized by western blotting with an anti-FLAG antibody (Sigma).

3. Results

3.1. Overall crystal structure of the TRIM75 coiled-coil domain

TRIM75 is a member of the subfamily containing RING domain, B box 2 domain, coiled-coil domain and B30.2/SPRY domain (Fig. 1). The coiled-coil domain of TRIM75, consisting of residues 168–222, was crystallized (Fig. 2A). The crystal structure was solved at 2.05 Å by molecular replacement, with one molecule in the asymmetric unit of space group *I*4122. The statistics of data collection and refinement are shown in Table 1. The monomer structure indicates that this protein forms an alpha helix with a slight bend (Fig. 2B). The symmetric analysis clearly shows that four symmetrically associated chains are closely packed together to form a tetramer (Fig. 2C). Among these, two chains (green and cyan) form one antiparallel dimer, and the other two chains (magenta and brown) form the other antiparallel dimer. The two dimers crossed each other at a crossing angle of approximately 26° to form a tetramer.

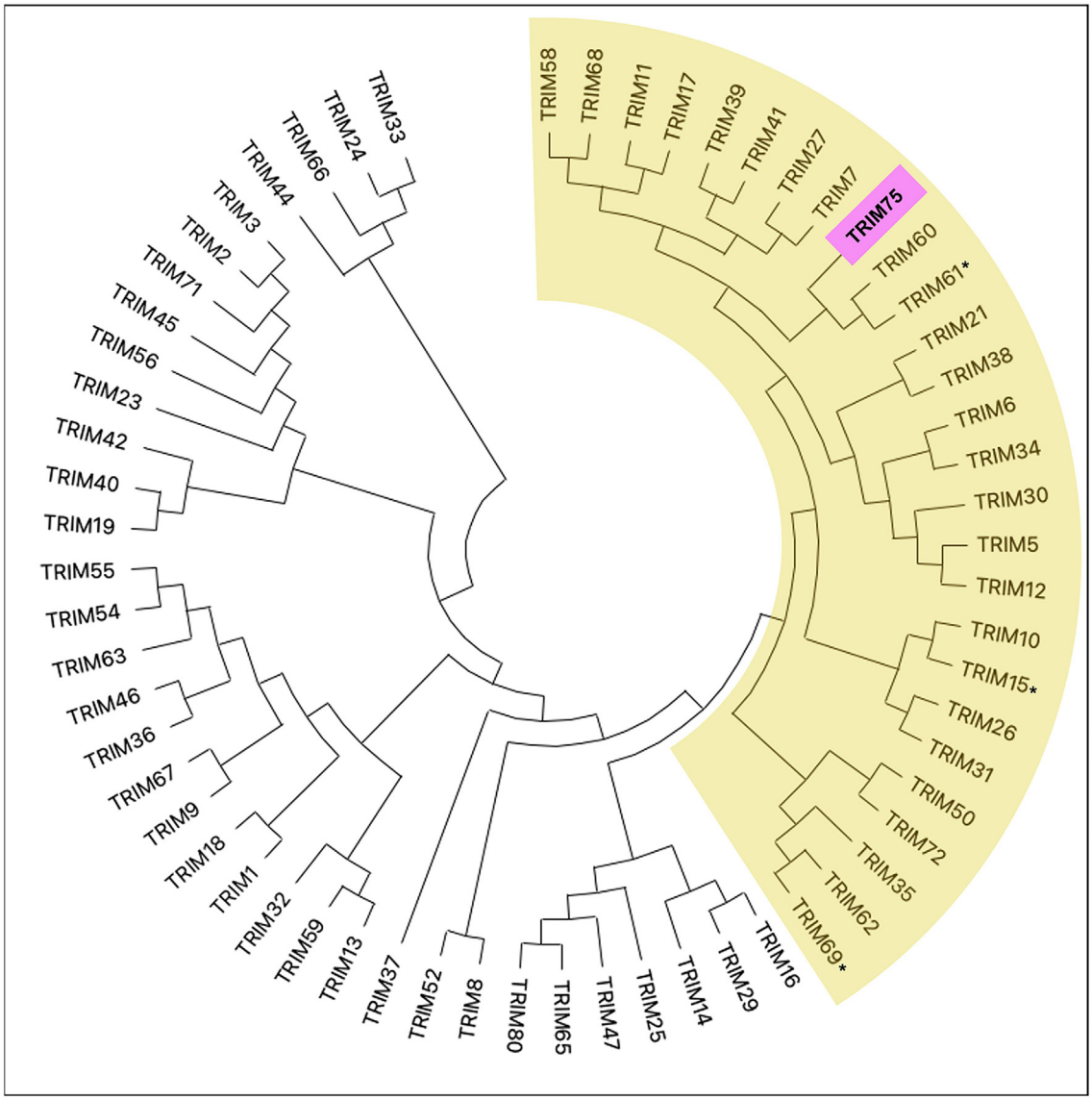

Fig. 1. Phylogenetic analysis of mouse TRIM proteins. The branch containing RING domain, B box 2 domain, coiled coil domain and B30.2/SPRY domain is shaded in yellow. The TRIM75 is highlighted in pink. The phylogenetic tree was constructed using MEGA 11 software. *Note that TRIM15 has no B30.2/SPRY domain; TRIM61 and TRIM69 have no B box 2 domain. (For interpretation of the references to colour in this figure legend, the reader is referred to the web version of this article.)

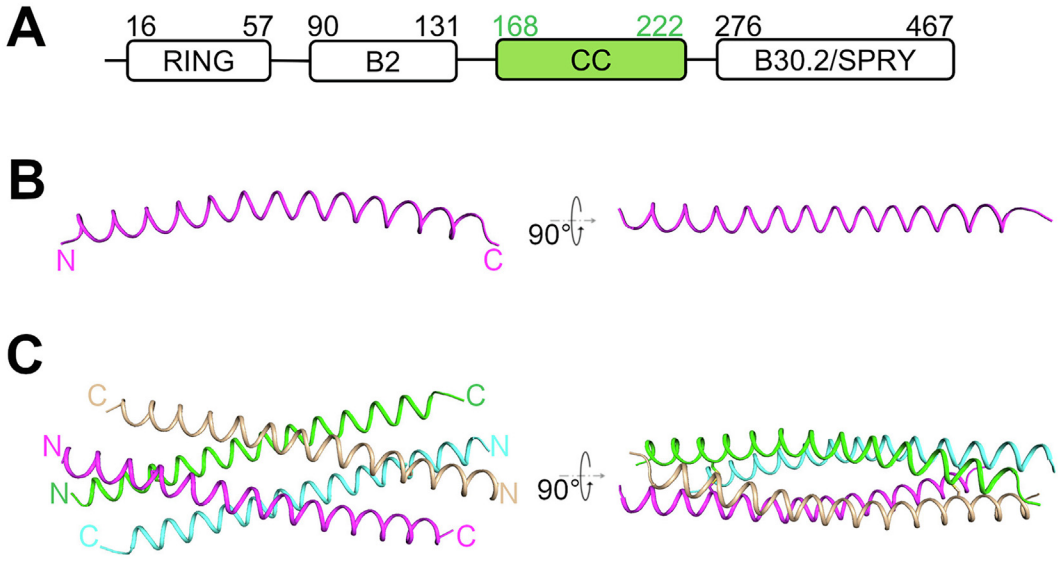

Fig. 2. Overall crystal structure of the TRIM75 coiled-coil domain. (A) Schematic representation of TRIM75 domain organization. B2, B box 2; CC, the coiled-coil domain. The residue boundaries of the domains are indicated. The coiled-coil domain is highlighted in green. (B, C) Cartoon representation of (B) a molecule in the asymmetric unit, and (C) a tetramer in two vertical views. (For interpretation of the references to colour in this figure legend, the reader is referred to the web version of this article.)

3.2. Protein-protein interactions involved in TRIM75 tetramerization

The interactions between the two antiparallel chains were then analyzed. The results indicated the existence of hydrophobic residues, salt bridges, and hydrogen bonds at the dimerization interface (Fig. 3). There are three hydrophobic regions: one is contributed by the side chains of F200 in the middle of the two chains; the other two symmetrically associated regions are contributed by C185 and the side chain of M189 from one chain and the side chain of M215 from the other chain. Further, four interchain salt bridges, including two formed between E186 and K212 and the other two formed between R197 and D205, as well as two symmetrically associated hydrogen bonds between the side chain of D193 and that of E211, also exist at the interface. Overall, these interactions contribute to the dimerization of the two antiparallel chains.

The two antiparallel dimers continue to bind together at a small crossing angle to form a tetramer. Structural analysis indicated the existence of several types of interactions between the two dimers for tetramerization. To better illustrate these interactions, five independent interaction regions were marked with different shapes (Fig. 4). In the cyan trapezoid-marked region, the side chains of I218, L215, L214, and L210 on the cyan-colored molecule, the side chain of M189 on the green-colored molecule, and the side chains of L188, F191, and L192 on the magenta-colored molecule form hydrophobic interactions (Fig. 4A). In the orange diamond-marked region, one hydrogen bond exists between the side chain of E211 on the cyan-colored molecule and that of E196 on the magenta-colored molecule (Fig. 4B). In the black oval marked region, two interchain salt bridges are formed between Q177 and R178, and the side chains of L181 from both chains contribute to the hydrophobic interaction (Fig. 4C). In the central region marked by the black rectangle, the side chains of L203 and F200 from the four chains form a central hydrophobic interaction (Fig. 4D). In the cycle-marked position, two Cysteines (C185), one from the magenta-colored chain and the other from the green-colored chain, form a disulfide bond (Fig. 5A). The interchain disulfide bond was further confirmed by the 2Fo-Fc omit electron density map (Fig. 5A) and reducing/non-reducing SDS-PAGE (Fig. 5B). Owing to the existence of symmetry, the interactions shown in the oval and the cycle-marked regions also exist in their symmetric regions in the tetramer; the interactions shown in the trapezoid and the diamond-marked regions also exist in the other three symmetri-

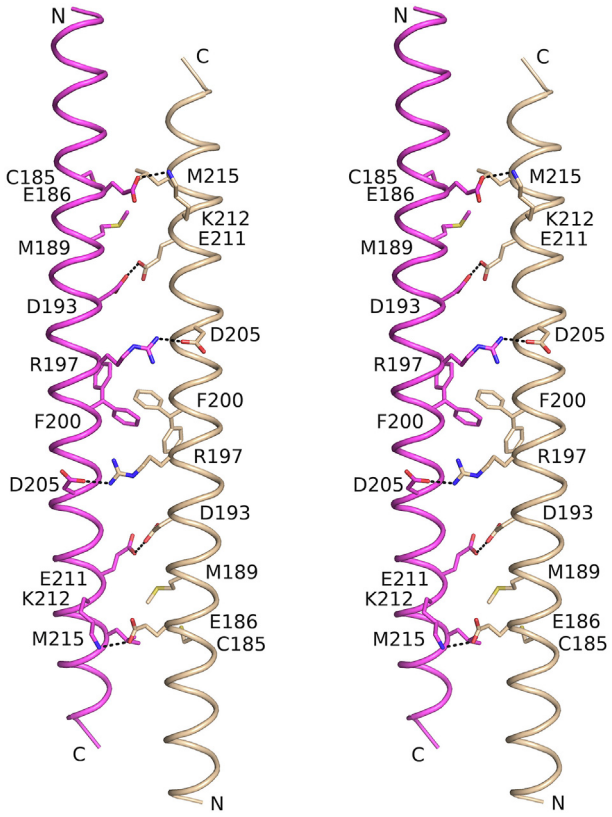

Fig. 3. Stereo view of the interactions between two antiparallel helices. The two antiparallel helices colored magenta and brown in Fig. 2 are shown as a ribbon diagram. The side chains of the residues involved in dimerization are presented as sticks. Salt bridges and hydrogen bonds are indicated by black dashed lines. (For interpretation of the references to colour in this figure legend, the reader is referred to the web version of this article.)

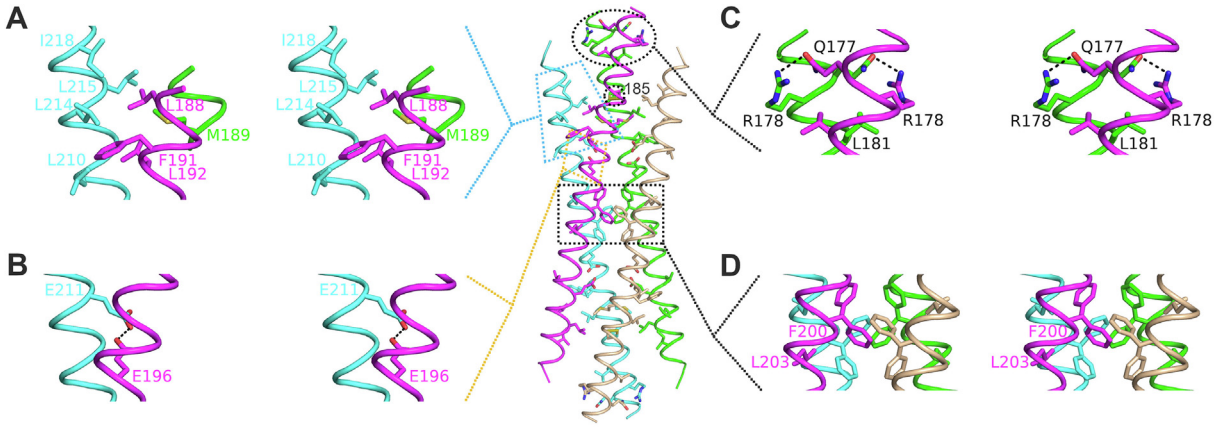

Fig. 4. Protein-protein interactions between two dimers for tetramerization. The interactions are divided into five independent regions, marked with different shapes. The enlarged views of the regions marked the (A) trapezoid, (B) diamond, (C) oval, and (D) rectangle are shown in stereo as cross-eye pairs. The side chains of the interacting residues are presented as sticks. Salt bridges and hydrogen bonds are indicated by black dashed lines.

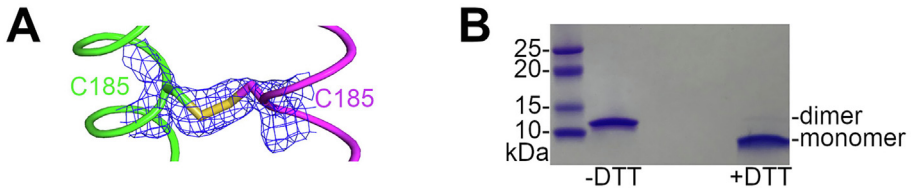

Fig. 5. Identification of interchain disulfide bonds. (A) The 2Fo-Fc omit map of the disulfide bond contoured at 1.5σ. (B) SDS-PAGE analysis of disulfide bond formation between two dimers. The purified protein was electrophoresed in non-reducing (−DTT) and reducing (+DTT) SDS-PAGE. The gel was stained with Coomassie Brilliant Blue. Molecular weight markers are indicated on the left. (For interpretation of the references to colour in this figure legend, the reader is referred to the web version of this article.)

cally associated regions. The two dimers can bind together to form a stable tetramer through these interactions.

3.3. Oligomeric assembly in solution

To investigate the oligomeric state of the purified coiled-coil protein, SEC-MALS was used to determine the absolute molar mass of the sample, and a glutaraldehyde chemical crosslink was used to analyze its oligomer, wherein glutaraldehyde was used as a small cross-linker that may covalently link two close protein molecules. The SEC-MALS result indicated that the purified coiled-coil domain existed as a tetramer in PBS solution (Fig. 6A). Glutaraldehyde chemical cross-linking confirmed the tetramer presence in the purified coiled-coil protein (Fig. 6B). Furthermore, the assembly state of intracellular expressed full-length proteins was analyzed by a chemical cross-linking experiment. In this experiment, a clear tetramer band was detected for the full-length protein expressed in HEK293T cells (Fig. 6C). To investigate the role of disulfide bonds in tetramer stability, the coiled-coil protein was further analyzed while in PBS with 5 mM DTT. The results of the SEC-MALS experiment showed that the protein failed to form stable tetramers in the presence of 5 mM DTT (Fig. 6D), and only one weak tetramer band was detected in the crosslinking experiment under reduced conditions (Fig. 6E). Cross-linking experiments of the full-length protein with a C185A mutation expressed in HEK293T cells showed that the tetrameric state was compromised when compared to that of wild type full length protein (Fig. 6F). Therefore, the disulfide bonds play a critical role in tetramer stability. To further determine the role of the proposed coiled-coil interface during tetramerization of the full protein, nine critical residues (Q177, R178, L181, C185, L188, F191, L192, E196, L203) involved the tetramerization (Fig. 4) were mutated to alanine. This mutation is indicated by CCm9A in the following sections. The SEC-MALS and crosslinking experiments revealed that the coiled-coil domain with the CCm9A mutation only formed dimers in PBS solution (Fig. 6G and 6H). When full-length protein with the CCm9A mutation was expressed in HEK293T cells, no clear tetramer band was detected (Fig. 6I). These results indicate that the proposed coiled-coil interface is responsible for the tetramer assembly.

3.4. Structural comparisons with other known TRIM coiled-coil structures

Structural studies indicated that TRIM fragments containing coiled-coil domain and part of C-terminal domain may form antiparallel dimers [16–20]. Among these structures, short helical segments from the C-terminal portion may pack against the center region of the coiled-coil domains. After superposing the TRIM75 tetrameric structure onto TRIM5 (PDB code: 4TN3), TRIM20 (PDB code: 4CG4), TRIM25 (PDB code: 4LTB), and TRIM69 (PDB code: 4NQJ) dimer structures, we observed that the short helical segments from C-terminal region bind on the same face as the tetramerization interface in the TRIM75 structure (Fig. 7-A-7D). This binding is mostly mediated by hydrophobic interactions. This face is termed "the hydrophobic face" in the following sections. The sequence alignment indicated that: (1) the center of the coiled coil domain consists of hydrophobic residues, and these residues locate on "the hydrophobic face"; and (2) there are ample hydrophobic residues located at other positions on "the hydrophobic face" for all the five structures (Fig. 7E). Although cystine doesn't exist in the four known structures, cystines exist at the same position for TRIM61 and TRIM40, and "the hydrophobic face" of several other TRIM members (Fig. S1). Due to the existence of a twofold axis perpendicular to "the hydrophobic face" at the center of the coiled-coil dimer based on TRIM75 structure (Fig. 3) and the other four known

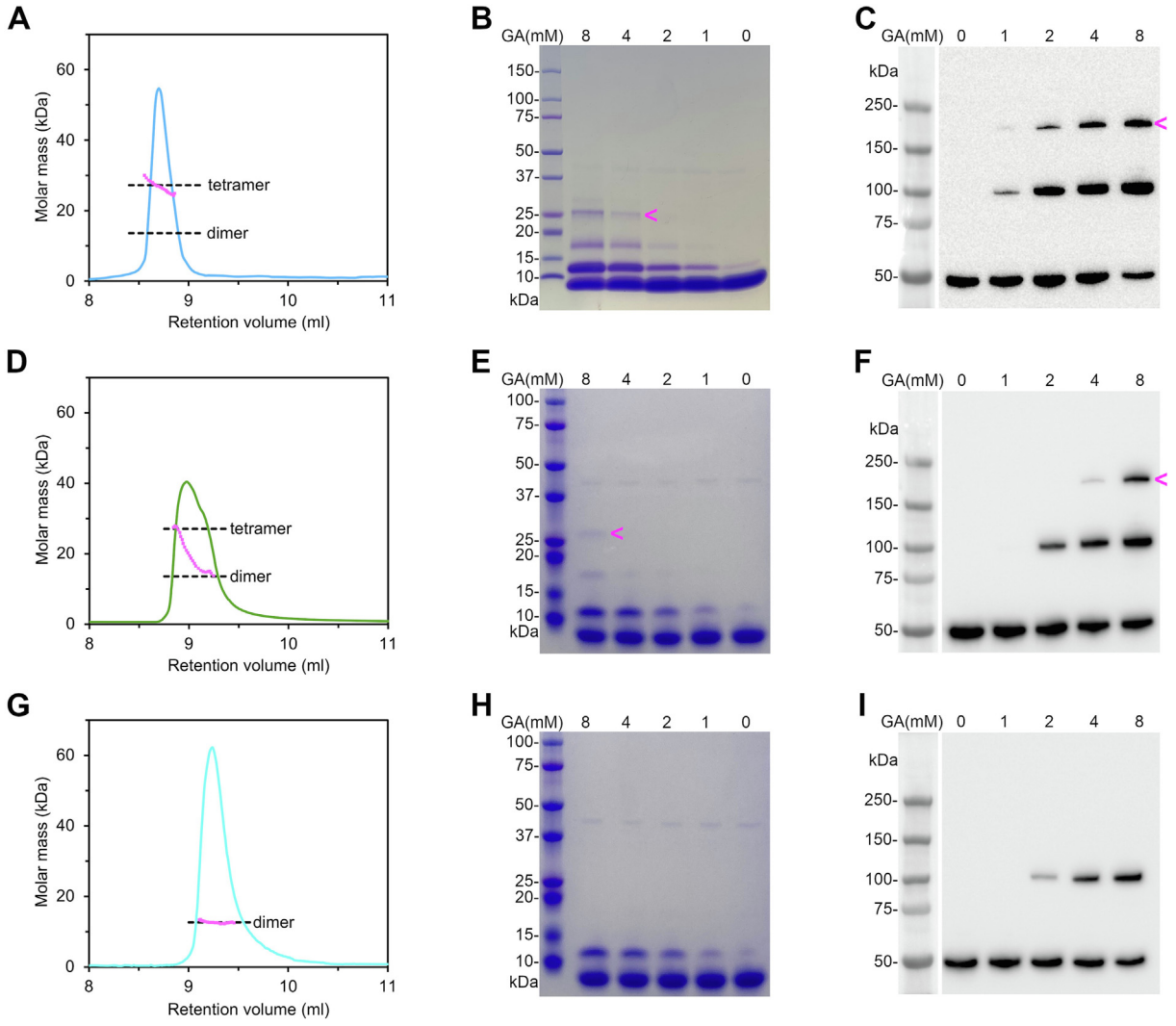

Fig. 6. Assembly analysis of TRIM75 in solution. (A) Oligomerization analysis of the purified TRIM75 coiled-coil domain using SEC-MALS. The measured molar mass of the peak is shown in magenta. The dimer (13.62 kDa) and tetramer (27.24 kDa) masses calculated from the protein sequence are indicated with black dashed lines. (B) Cross-linking analysis of the purified coiled-coil domain. Molecular weight markers are indicated on the left of the panel. The concentrations of glutaraldehyde (GA) are indicated at the top of the panel. The predicted tetramer is indicated by a magenta arrow. (C) Cross-linking analysis of the full-length protein expressed in HEK293T cells. (D) SEC-MALS analysis of TRIM75 coiled-coil domain under reducing conditions. The elution buffer is PBS with 5 mM DTT. (E) Cross-linking analysis of the purified coiled-coil domain under reducing conditions. The protein was in PBS with 5 mM DTT. (F) Cross-linking analysis of the full-length protein of the C185A mutant expressed in HEK293T cells. (G) SEC-MALS analysis of the TRIM75 coiled-coil domain with the CCm9A mutation. The dimer mass (12.66 kDa) is indicated with a black dashed line. (H) Cross-linking analysis of the coiled-coil domain with the CCm9A mutation. (I) Cross-linking analysis of the full-length protein with the CCm9A mutation expressed in HEK293T cells. (For interpretation of the references to colour in this figure legend, the reader is referred to the web version of this article.)

coiled-coil structures, any cystines or hydrophobic residues on "the hydrophobic face" would exist at symmetric positions on the same face. Therefore, this structure allows these cystines to form disulfide bonds, and hydrophobic residues to bind via hydrophobic interactions in space if two dimers may form an approximately antiparallel tetramer through the binding between "the hydrophobic face" of the two dimers. As for TRIM75, no hydrophobic residues were located on the back of the tetramer (Fig. S2). To investigate whether the C-terminal region in TRIM75 protein similarly binds on "the hydrophobic face" via hydrophobic interactions and affects the tetramerization, a truncated TRIM75 protein (136–467) containing the coiled coil and C-terminal domains was analyzed. Crosslinking experiment indicated that this truncated protein still may form tetramers (Fig. S3A), while no tetramer band was detected for the CCm9A version of this truncated protein (Fig. S3B). Therefore, the C-terminal region did not interfere with the tetramerization mediated by coiled-coil domain in the absent of *N*-terminal domain for TRIM75 protein.

3.5. Stable tetrameric model mediated by the coiled-coil domain

The two disulfide bonds, as well as other interactions, evidently link the two dimers covalently at a small crossing angle to form a stable tetramer. In this tetramer, the domains on the left side are twofold symmetric to those on the right side. Two *N*-terminals, including the RING domain and B box 2, and two C-terminals, including the B30.2/SPRY domain, are present on each side, as shown in the model (Fig. 8). The two *N*-terminals on the same side are close in space; therefore, it is favorable for the two B box 2 domains linked to the coiled-coil domain to form a homodimer. Similarly, the two RING domains linked to B box 2 on the same side can also form a homodimer. Once the RING dimer is formed, the dimerized RING domain can recruit the E2-Ub complex and trans-

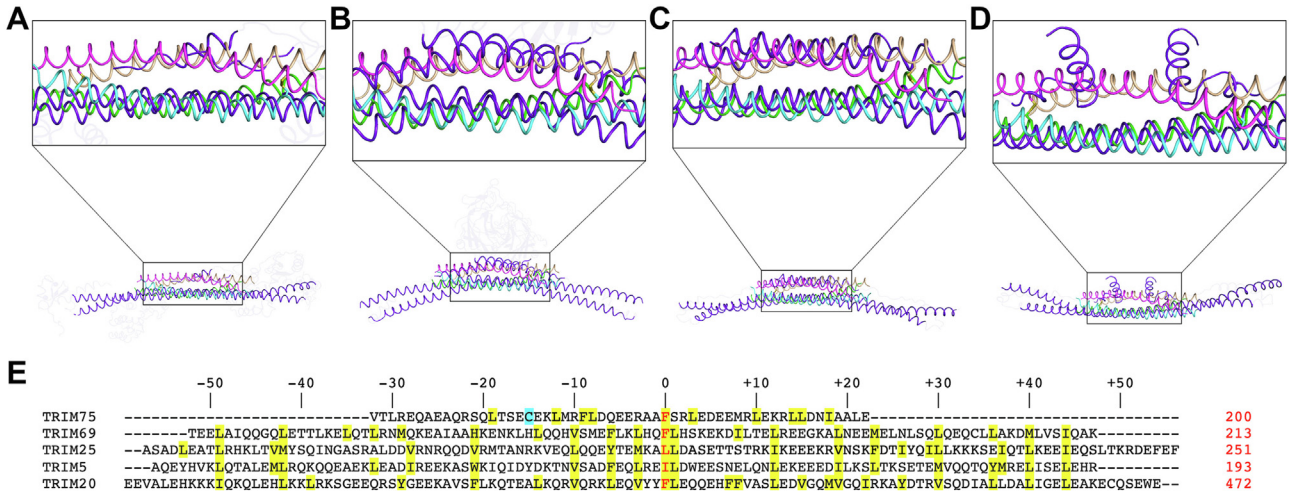

Fig. 7. Structural comparison between **TRIM75 coiled-coil domain and other four known coiled-coil structures.** One dimer of TRIM75 was separately superposed on the coiled coil domain of (A) TRIM5, (B) TRIM20, (C) TRIM25 and (D) TRIM 69. The center regions of the coiled-coil structures are magnified. The TRIM75 tetramer (in green, cyan, magenta, and brown), coiled-coiled domain and helices covering the center region of the coiled-coil domain from target structures (in purple) are highlighted. Other regions of the structures are set to transparent for clarity. (E) Sequence alignment of the five structures. The center residues of their coiled coil structures are shown in red, and their residue positions are shown in red to the right of their sequences. The relative positions to the center residues are shown at the top. Hydrophobic residues located on "the hydrophobic face" are shaded in yellow. The cystine is shaded in cyan. (For interpretation of the references to colour in this figure legend, the reader is referred to the web version of this article.)

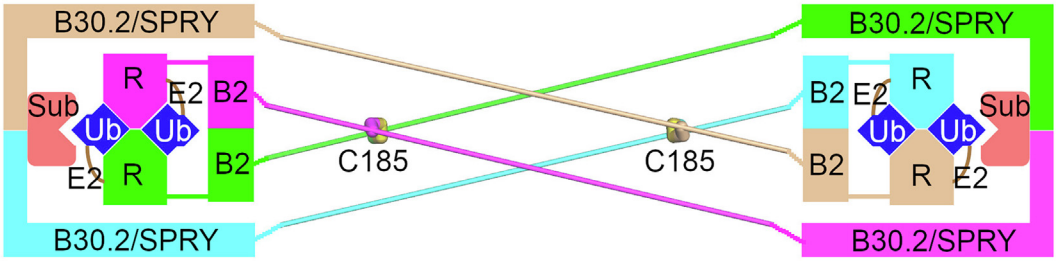

Fig. 8. Coiled-coil domain-mediated tetrameric model of TRIM E3 ligases. In this model, two antiparallel coiled-coil dimers in a cylinder representation are bound together with a small crossing angle (~26°) and are covalently linked by two interchain disulfide bonds mediated by C185 residues. This stable tetrameric architecture allows dimerization of two B2 boxes and two RING domains located on the same side. One active RING dimer binds to two E2-Ub. Two C-terminal domains (B30.2/SPRY) exist on the same side and can present a substrate (Sub) to a close E2-Ub complex.

fer ubiquitin from the E2 enzyme to the protein substrate recruited by the C-terminal B30.2/SPRY domain on the same side. Therefore, the tetrameric model derived from the stable coiled-coil domain provides a reasonable mechanistic explanation of the mechanism by which the TRIM protein assembles to exert its ubiquitin E3 ligase activity.

4. Discussion

4.1. TRIM75 coiled-coil domain forms a tetramer

RING-type E3 ligases can catalyze the direct transfer of ubiquitin from the E2 enzyme to specific substrates [29,30]. To achieve this function, the RING domain must form an active dimer; meanwhile, the recruited E2-Ub complex and substrate should be close enough to fulfill the direct transfer. Therefore, a suitable assembly and rational spatial arrangement of domains are crucial for the E3 ligase activities of these proteins.

As the largest family of RING E3 ligases, TRIM members have a characteristic domain organization, containing the RING domain, B box(s), coiled-coil domain, and variable C-terminal domain. The coiled-coil domain may form an antiparallel dimer [16–20], where the two RING domains located at opposite ends are inactive monomers. This raises the question of how TRIM proteins assemble to satisfy the dimerization of the RING domain. Here, we exhibit that in TRIM75, the coiled-coil domain alone may form a tetrameric assembly. Two disulfide bonds are involved during the tetramerization of the coiled-coil domain. Owing to the covalent links, the CC tetramer should be stable enough to maintain the tetramerization of the full-length protein.

4.2. Tetrameric structure facilitates direct ubiquitin transfer

The coiled-coil tetrameric structure brings two *N*-terminal domains on the same side close enough for spatial contact and facilitates RING dimerization. Although structural information is not available for the RING domain and B box 2 of TRIM75, dimerized crystal or NMR structures of *N*-terminal domains have been reported in other TRIM members, including the RING domain of TRIM69 [31], TRIM32 [32], and TRIM37 (PDB ID:3LRQ); B box 2 of TRIM63 [33], TRIM54 (PDB ID:3Q1D), and TRIM28 (PDB ID:2YVR); B box 1 of TRIM19 [34] and TRIM28 [35]; and RING combined with B box 2 of TRIM21 [36]. This suggests that the tetramer is a suitable assembly to facilitate RING dimer formation. The tetrameric structure also provides proximity to the recruited E2-Ub and substrate to accomplish the direct transfer of ubiquitin. As the tetramer may well satisfy the two critical prerequisites for TRIM members exerting their E3 ligase activities, a strategy that

regulates the coiled-coil tetramer may facilitate the controlled formation of the activated structure, thereby affecting the TRIM E3 ligase activity. Examples including influenza A virus nonstructural protein 1 (NS1) inhibiting TRIM25 function in ubiquitinating RIG-1 pathway [19,37] and IE1 protein suppressing TRIM19 activities seem to support this inference [38,39].

4.3. Cooperative interactions promote TRIM protein tetramerization

Once the coiled-coil domain forms a tetramer, as shown in the model, two *N*-terminal domains are located on each side of the coiled-coil tetramer. The tetrameric architecture facilitates the dimerization of *N*-terminal domains on the same side. The dimerization interaction of two RING domains on each side can generate binding affinity, similar to the two B boxes. Therefore, five binding interactions are present in the model: two from the dimerization of the RING domain, two from the dimerization of the B box, and one from the tetramerization of the coiled-coil domain. All five binding interactions may cooperatively promote the tetramerization of the full-length protein. For TRIM75, the tetramer of the coiled-coil domain is stable because of the two disulfide bonds; thus, the binding affinity contributed by the other four binding interactions may not be required for maintaining the tetramer of the full-length protein. In other members, the cooperative interactions contributed by other domains may be required to maintain the tetramerization of full-length proteins in the absence of strong interactions. This may explain the oligomeric states of some reported TRIM members. For example, B-box 2 promotes higher-order oligomerization of TRIM5 protein to exert its ubiquitin E3 ligase activity; the combined fragment containing B box2 and the coiled-coil domain form a higher-order assembly for TRIM63 [33]; the B box and coiled-coil domain together promote TRIM27 multimerization [40]; and the TRIM32 fragment containing the RING domain, B box 2, and the coiled-coil domain presents an elongated tetramer profile in a small-angle X-ray scattering (SAXS) experiment [32]. In theory, two dimers could possibly bind through the dimerization of only one *N*-terminal domain; another *N*-terminal domain participates in dimerization with the *N*-terminal domain from a third dimer. Through this interaction, TRIM can be continually elongated by binding more dimers to form multiple aggregates. Compared to tetramerization with the five binding interactions shown in the present model, linear aggregation with only two binding interactions is relatively weaker.

In summary, this study illustrates that the coiled-coil domain of TRIM75, a member of the largest family of RING E3 ligases, forms a tetrameric structure wherein two interchain disulfide bonds are involved in tetramerization. This unique interaction allows TRIM75 to form a stable tetramer. Such a structure permits the formation of an active RING dimer and satisfies the spatial arrangement for direct transfer of ubiquitin groups from the E2 enzyme to the substrates. Clearly, this model is derived from the structure of the coiled coil domain; therefore, full-length protein structure obtained with new technology will provide more comprehensive evidence. Overall, this structural model may represent the tetrameric architecture of TRIM functions and provide novel insights into the mechanism of action of TRIM E3 ligases, including their ubiquitination mechanism and potential therapeutic strategies in RING E3 ligase-associated diseases.

5. Accession numbers

The atomic coordinates and structure factors have been deposited in the Protein Data Bank (https://www.wwpdb.org) with the access code 7UG2.

Declaration of Competing Interest

The authors declare that they have no known competing financial interests or personal relationships that could have appeared to influence the work reported in this paper.

Acknowledgments

We thank Biomolecular Structure and Function Core in MD Anderson Cancer Center for providing SEC-MALS analysis. This research used resources of the Advanced Photon Source, a U.S. Department of Energy (DOE) Office of Science User Facility operated for the DOE Office of Science by Argonne National Laboratory under Contract No. DE-AC02-06CH11357. This project was supported in part by the NIH grants R01 AI080779 and R01 AI155488.

Appendix A. Supplementary data

Supplementary data to this article can be found online at https://doi.org/10.1016/j.csbj.2022.08.069.

References

[1] Komander D, Rape M. The ubiquitin code. Annu Rev Biochem 2012;81:203–29. https://doi.org/10.1146/annurev-biochem-060310-170328.
[2] Glickman MH, Ciechanover A. The ubiquitin-proteasome proteolytic pathway: destruction for the sake of construction. Physiol Rev 2002;82:373–428. https://doi.org/10.1152/physrev.00027.2001.
[3] Mukhopadhyay D, Riezman H. Proteasome-independent functions of ubiquitin in endocytosis and signaling. Science 2007;315:201–5. https://doi.org/10.1126/science.1127085.
[4] Morreale FE, Walden H. Types of Ubiquitin Ligases. Cell 2016;165:248–248.e1. https://doi.org/10.1016/j.cell.2016.03.003.
[5] Plechanovová A, Jaffray EG, Tatham MH, Naismith JH, Hay RT. Structure of a RING E3 ligase and ubiquitin-loaded E2 primed for catalysis. Nature 2012;489:115–20. https://doi.org/10.1038/nature11376.
[6] Buetow L, Huang DT. Structural insights into the catalysis and regulation of E3 ubiquitin ligases. Nat Rev Mol Cell Biol 2016;17:626–42. https://doi.org/10.1038/nrm.2016.91.
[7] van Gent M, Sparrer KMJ, Gack MU. TRIM Proteins and Their Roles in Antiviral Host Defenses. Annu Rev Virol 2018;5:385–405. https://doi.org/10.1146/annurev-virology-092917-043323.
[8] Ozato K, Shin D-M, Chang T-H, Morse HC. TRIM family proteins and their emerging roles in innate immunity. Nat Rev Immunol 2008;8:849–60. https://doi.org/10.1038/nri2413.
[9] Hatakeyama S. TRIM Family Proteins: Roles in Autophagy, Immunity, and Carcinogenesis. Trends Biochem Sci 2017;42:297–311. https://doi.org/10.1016/j.tibs.2017.01.002.
[10] Watanabe M, Hatakeyama S. TRIM proteins and diseases. J Biochem (Tokyo) 2017;161:135–44. https://doi.org/10.1093/jb/mvw087.
[11] Zhang J, Li X, Hu W, Li C. Emerging Role of TRIM Family Proteins in Cardiovascular Disease. Cardiology 2020;145:390–400. https://doi.org/10.1159/000506150.
[12] Hatakeyama S. TRIM proteins and cancer. Nat Rev Cancer 2011;11:792–804. https://doi.org/10.1038/nrc3139.
[13] Kiss L, Zeng J, Dickson CF, Mallery DL, Yang J-C, McLaughlin SH, et al. A tri-ionic anchor mechanism drives Ube2N-specific recruitment and K63-chain ubiquitination in TRIM ligases. Nat Commun 2019;10:4502. https://doi.org/10.1038/s41467-019-12388-y.
[14] Dawidziak DM, Sanchez JG, Wagner JM, Ganser-Pornillos BK, Pornillos O. Structure and catalytic activation of the TRIM23 RING E3 ubiquitin ligase. Proteins 2017;85:1957–61. https://doi.org/10.1002/prot.25348.
[15] Anandapadamanaban M, Kyriakidis NC, Csizmók V, Wallenhammar A, Espinosa AC, Ahlner A, et al. E3 ubiquitin-protein ligase TRIM21-mediated lysine capture by UBE2E1 reveals substrate-targeting mode of a ubiquitin-conjugating E2. J Biol Chem 2019;294:11404–19. https://doi.org/10.1074/jbc.RA119.008485.
[16] Goldstone DC, Walker PA, Calder LJ, Coombs PJ, Kirkpatrick J, Ball NJ, et al. Structural studies of postentry restriction factors reveal antiparallel dimers that enable avid binding to the HIV-1 capsid lattice. Proc Natl Acad Sci U S A 2014;111:9609–14. https://doi.org/10.1073/pnas.1402448111.
[17] Weinert C, Morger D, Djekic A, Grütter MG, Mittl PRE. Crystal structure of TRIM20 C-terminal coiled-coil/B30.2 fragment: implications for the recognition of higher order oligomers. Sci Rep 2015;5:10819. https://doi.org/10.1038/srep10819.
[18] Sanchez JG, Okreglicka K, Chandrasekaran V, Welker JM, Sundquist WI, Pornillos O. The tripartite motif coiled-coil is an elongated antiparallel hairpin dimer. Proc Natl Acad Sci U S A 2014;111:2494–9. https://doi.org/10.1073/pnas.1318962111.

[19] Koliopoulos MG, Lethier M, van der Veen AG, Haubrich K, Hennig J, Kowalinski E, et al. Molecular mechanism of influenza A NS1-mediated TRIM25 recognition and inhibition. Nat Commun 2018;9:1820. https://doi.org/10.1038/s41467-018-04214-8.
[20] Li Y, Wu H, Wu W, Zhuo W, Liu W, Zhang Y, et al. Structural insights into the TRIM family of ubiquitin E3 ligases. Cell Res 2014;24:762–5. https://doi.org/10.1038/cr.2014.46.
[21] Tamura K, Stecher G, Kumar S. MEGA11: Molecular Evolutionary Genetics Analysis Version 11. Mol Biol Evol 2021;38:3022–7. https://doi.org/10.1093/molbev/msab120.
[22] Battye TGG, Kontogiannis L, Johnson O, Powell HR, Leslie AGW. iMOSFLM: a new graphical interface for diffraction-image processing with MOSFLM. Acta Crystallogr D Biol Crystallogr 2011;67:271–81. https://doi.org/10.1107/S0907444910048675.
[23] Winn MD, Ballard CC, Cowtan KD, Dodson EJ, Emsley P, Evans PR, et al. Overview of the CCP4 suite and current developments. Acta Crystallogr D Biol Crystallogr 2011;67:235–42. https://doi.org/10.1107/S0907444910045749.
[24] McCoy AJ, Grosse-Kunstleve RW, Adams PD, Winn MD, Storoni LC, Read RJ. Phaser crystallographic software. J Appl Crystallogr 2007;40:658–74. https://doi.org/10.1107/S0021889807021206.
[25] Murshudov GN, Skubák P, Lebedev AA, Pannu NS, Steiner RA, Nicholls RA, et al. REFMAC5 for the refinement of macromolecular crystal structures. Acta Crystallogr D Biol Crystallogr 2011;67:355–67. https://doi.org/10.1107/S0907444911001314.
[26] Emsley P, Cowtan K. Coot: model-building tools for molecular graphics. Acta Crystallogr D Biol Crystallogr 2004;60:2126–32. https://doi.org/10.1107/S0907444904019158.
[27] Li X, Sodroski J. The TRIM5α B-Box 2 Domain Promotes Cooperative Binding to the Retroviral Capsid by Mediating Higher-Order Self-Association. J Virol 2008;82:11495–502. https://doi.org/10.1128/JVI.01548-08.
[28] Javanbakht H, Yuan W, Yeung DF, Song B, Diaz-Griffero F, Li Y, et al. Characterization of TRIM5alpha trimerization and its contribution to human immunodeficiency virus capsid binding. Virology 2006;353:234–46. https://doi.org/10.1016/j.virol.2006.05.017.
[29] Metzger MB, Pruneda JN, Klevit RE, Weissman AM. RING-type E3 ligases: master manipulators of E2 ubiquitin-conjugating enzymes and ubiquitination. Biochim Biophys Acta 2014;1843:47–60. https://doi.org/10.1016/j.bbamcr.2013.05.026.
[30] Berndsen CE, Wolberger C. New insights into ubiquitin E3 ligase mechanism. Nat Struct Mol Biol 2014;21:301–7. https://doi.org/10.1038/nsmb.2780.
[31] Keown JR, Yang J, Black MM, Goldstone DC. The RING domain of TRIM69 promotes higher-order assembly. Acta Crystallogr Sect Struct Biol 2020;76:954–61. https://doi.org/10.1107/S2059798320010499.
[32] Koliopoulos MG, Esposito D, Christodoulou E, Taylor IA, Rittinger K. Functional role of TRIM E3 ligase oligomerization and regulation of catalytic activity. EMBO J 2016;35:1204–18. , https://doi.org/10.15252/embj.201593741.
[33] Mrosek M, Meier S, Ucurum-Fotiadis Z, von Castelmur E, Hedbom E, Lustig A, et al. Structural analysis of B-Box 2 from MuRF1: identification of a novel self-association pattern in a RING-like fold. Biochemistry 2008;47:10722–30. https://doi.org/10.1021/bi800733z.
[34] Huang S-Y, Naik MT, Chang C-F, Fang P-J, Wang Y-H, Shih H-M, et al. The B-box 1 dimer of human promyelocytic leukemia protein. J Biomol NMR 2014;60:275–81. https://doi.org/10.1007/s10858-014-9869-4.
[35] Sun Y, Keown JR, Black MM, Raclot C, Demarais N, Trono D, et al. A Dissection of Oligomerization by the TRIM28 Tripartite Motif and the Interaction with Members of the Krab-ZFP Family. J Mol Biol 2019;431:2511–27. https://doi.org/10.1016/j.jmb.2019.05.002.
[36] Dickson C, Fletcher AJ, Vaysburd M, Yang J-C, Mallery DL, Zeng J, et al. Intracellular antibody signalling is regulated by phosphorylation of the Fc receptor TRIM21. ELife 2018;7:e32660.
[37] Gack MU, Albrecht RA, Urano T, Inn K-S, Huang I-C, Carnero E, et al. Influenza A virus NS1 targets the ubiquitin ligase TRIM25 to evade recognition by the host viral RNA sensor RIG-I. Cell Host Microbe 2009;5:439–49. https://doi.org/10.1016/j.chom.2009.04.006.
[38] Kang H, Kim ET, Lee H-R, Park J-J, Go YY, Choi CY, et al. Inhibition of SUMO-independent PML oligomerization by the human cytomegalovirus IE1 protein. J Gen Virol 2006;87:2181–90. https://doi.org/10.1099/vir.0.81787-0.
[39] Scherer M, Klingl S, Sevvana M, Otto V, Schilling E-M, Stump JD, et al. Crystal Structure of Cytomegalovirus IE1 Protein Reveals Targeting of TRIM Family Member PML via Coiled-Coil Interactions. PLOS Pathog 2014;10:e1004512.
[40] Cao T, Borden KL, Freemont PS, Etkin LD. Involvement of the rfp tripartite motif in protein-protein interactions and subcellular distribution. J Cell Sci 1997;110 (Pt 14):1563–71.